

Direct capture cross section and resonances in the $^{22}\text{Ne}(p, \gamma)^{23}\text{Na}$ reaction at low energy

M. P. Takács,^{1,2,*} F. Ferraro,³ D. Piatti^{4,5,†} J. Skowronski,^{4,5} M. Aliotta,⁶ C. Ananna,^{7,8} L. Barbieri,⁶ F. Barile,^{9,10} D. Bemmerer,^{1,‡} A. Best,^{7,8} A. Boeltzig,¹ C. Brogini,⁵ C. G. Bruno,⁶ A. Cacioli,^{4,5} M. Campostrini,¹¹ F. Casaburo,^{12,13} F. Cavanna,¹⁴ G. F. Ciani,⁹ P. Colombetti,^{14,15} A. Compagnucci,^{3,16} P. Corvisiero,^{12,13} L. Csedreki,¹⁷ T. Davinson,⁶ D. Dell'Aquila,^{7,8} R. Depalo,^{18,19} A. Di Leva,^{7,8} Z. Elekes,^{17,20} A. Formicola,²¹ Zs. Fülöp,¹⁷ G. Gervino,^{14,15} R. M. Gesuè,^{3,16} A. Guglielmetti,^{18,19} C. Gustavino,²¹ Gy. Gyürky,¹⁷ G. Imbriani,^{7,8} M. Junker,³ A. Karakas,²² M. Lugaro,^{23,24} P. Marigo,^{4,5} J. Marsh,⁶ E. Masha,^{1,18,19} R. Menegazzo,⁵ D. Mercogliano,^{7,8} V. Paticchio,⁹ P. Prati,^{12,13} D. Rapagnani,^{7,8} V. Rigato,¹¹ D. Robb,⁶ L. Schiavulli,^{9,10} R. S. Sidhu,⁶ O. Straniero,^{25,21} T. Szücs,¹⁷ and S. Zavatarelli^{13,12}
(LUNA Collaboration)

¹*Helmholtz-Zentrum Dresden-Rossendorf, Bautzner Landstraße 400, 01328 Dresden, Germany*

²*Technische Universität Dresden, Institut für Kern- und Teilchenphysik, Zellescher Weg 19, 01069 Dresden, Germany*

³*INFN Laboratori Nazionali del Gran Sasso (LNGS), 67100 Assergi (AQ), Italy*

⁴*Università degli Studi di Padova, Dipartimento di Fisica e Astronomia "G. Galilei", Via F. Marzolo 8, 35131 Padova, Italy*

⁵*INFN, Sezione di Padova, Via F. Marzolo 8, 35131 Padova, Italy*

⁶*SUPA, School of Physics and Astronomy, University of Edinburgh, EH9 3FD Edinburgh, United Kingdom*

⁷*Università degli Studi di Napoli "Federico II", Dipartimento di Fisica "E. Pancini", Via Cintia, 80126 Napoli, Italy*

⁸*INFN, Sezione di Napoli, Via Cintia, 80126 Napoli, Italy*

⁹*INFN, Sezione di Bari, 70125 Bari, Italy*

¹⁰*Università degli Studi di Bari, 70125 Bari, Italy*

¹¹*INFN Laboratori Nazionali di Legnaro, Via dell'Università 2, 35020 Legnaro (PD), Italy*

¹²*Università degli Studi di Genova, Via Dodecaneso 33, 16146 Genova, Italy*

¹³*INFN, Sezione di Genova, Via Dodecaneso 33, 16146 Genova, Italy*

¹⁴*INFN, Sezione di Torino, Via P. Giuria 1, 10125 Torino, Italy*

¹⁵*Università degli Studi di Torino, Via P. Giuria 1, 10125 Torino, Italy*

¹⁶*Gran Sasso Science Institute, 67100 L'Aquila, Italy*

¹⁷*HUN-REN Institute for Nuclear Research (HUN-REN ATOMKI), P.O. Box 51, H-4001 Debrecen, Hungary*

¹⁸*Università degli Studi di Milano, Via G. Celoria 16, 20133 Milano, Italy*

¹⁹*INFN, Sezione di Milano, Via G. Celoria 16, 20133 Milano, Italy*

²⁰*Institute of Physics, Faculty of Science and Technology, University of Debrecen, Egyetem tér 1, H-4032 Debrecen, Hungary*

²¹*INFN, Sezione di Roma La Sapienza, Piazzale A. Moro 2, 00185 Roma, Italy*

²²*Monash Centre for Astrophysics, School of Physics & Astronomy, Monash University, VIC 3800, Australia*

²³*Konkoly Observatory, Research Centre for Astronomy and Earth Sciences, Hungarian Academy of Sciences, 1121 Budapest, Hungary*

²⁴*ELTE Eötvös Loránd University, Institute of Physics, Budapest 1117, Pázmány Péter sétány 1/A, Hungary*

²⁵*INAF-Osservatorio Astronomico d'Abruzzo, Teramo, Italy*



(Received 24 August 2023; revised 21 December 2023; accepted 21 May 2024; published 28 June 2024)

Background: Among the several inhomogeneities in the composition of globular cluster stars, an overabundance of ^{23}Na is interpreted as the signature of the operation of the neon-sodium (NeNa) cycle. One of the hypothesis to explain the observed O-Na anticorrelation invokes massive asymptotic giant branch stars as the main agents. At temperatures relevant for nucleosynthesis in asymptotic giant branch stars the $^{22}\text{Ne}(p, \gamma)^{23}\text{Na}$ reaction rate has been the most uncertain so far, giving rise to considerable experimental efforts in recent years. While overall there is a good agreement between reported cross section results, some tensions still remain on the branching ratios of resonance γ -ray modes and direct capture to excited states.

Purpose: The present paper offers full details and a partial analysis of the high sensitivity study, of both direct capture and low-energy resonances in the $^{22}\text{Ne}(p, \gamma)^{23}\text{Na}$ reaction, performed at LUNA, and whose results were previously published in abbreviated form [F. Ferraro *et al.*, *Phys. Rev. Lett.* **121**, 172701 (2018)].

Methods: During the LUNA measurement an intense proton beam was delivered to a ^{22}Ne gas target. The γ rays from the $^{22}\text{Ne}(p, \gamma)^{23}\text{Na}$ reaction were detected by a high efficiency 4π , sixfold segmented bismuth germanate

*Present address: Physikalisch-Technische Bundesanstalt (PTB), Bundesallee 100, 38116, Braunschweig, Germany.

†Contact author: denise.piatti@pd.infn.it

‡Contact author: d.bemmerer@hzdr.de

(BGO) detector. In the present paper the data from individual detector segments were combined with simulated detector responses to obtain cascade branching ratios.

Results: For the three resonances at $E_p = 156.2$ and 259.7 keV new γ -decay branchings are provided. Moreover, partial cross sections for the direct capture to different states of ^{23}Na are reported down to $E_p = 188$ keV, the lowest energy measured to date.

Conclusions: A revised reaction rate has been calculated based on a new R -matrix fit of the recent $^{22}\text{Ne}(p, \gamma)^{23}\text{Na}$ S -factor data and results for the resonances. The thermonuclear reaction rate is provided in tabular form to be used in stellar models.

DOI: [10.1103/PhysRevC.109.064627](https://doi.org/10.1103/PhysRevC.109.064627)

I. INTRODUCTION

Hydrogen burning at temperatures as high as $T \approx 0.08$ – 0.1 GK, typical of hot bottom burning in asymptotic giant branch (HBB-AGB) stars, and as high as $0.15 < T < 0.45$ GK, typical of classical novae explosions, occur via both the CNO cycle and more advanced processes, such as the NeNa cycle [1,2]. While it contributes negligibly to the energy budget, the NeNa cycle is of great importance for stellar nucleosynthesis, because it affects the abundances of isotopes between ^{20}Ne and ^{24}Mg [3]. Predicting the sodium abundance observable in stellar atmospheres is, indeed, of great interest in the context of the longstanding puzzle of the Na-O anticorrelation in globular cluster (GC) stars [4,5]. This anomaly, together with other star-to-star abundance variations and independent photometric observations, are believed to indicate the presence of multiple populations of stars in GCs [5–7]. Particularly the increased abundance of ^{23}Na observed in some stars is interpreted as a signature of the operation of the NeNa cycle in previous stellar generations [8]. Different hypotheses for the origin of these anomalies have been investigated, such as mixing within the observed stars [9], pollution of the interstellar medium by previous stellar sources such as AGB stars [10], interactive binary systems [11], fast-rotating massive stars [12], supermassive stars [13], or several distinct stellar populations within a cluster [14].

In order to constrain one or more hypotheses, a comparison of predicted elemental abundances with increasingly precise observed values is needed. To this end, the uncertainties on the thermonuclear reaction rates of the processes involved should be reduced to a negligible level compared to stellar evolutionary aspects [3,15].

Until a few years ago, among the reactions of the NeNa cycle the $^{22}\text{Ne}(p, \gamma)^{23}\text{Na}$ (Q value = $8794.109(18)$ keV [16]) carried the largest uncertainty, with adopted reaction rates spanning up to three orders of magnitude at temperatures of interest [17,18]. Several sensitivity studies have investigated how such an uncertainty propagated to the abundances of intermediate-mass elements in AGB stars [3,15], showing yields variation up to two orders of magnitude [3], and classical novae explosions [19].

The large uncertainty of the $^{22}\text{Ne}(p, \gamma)^{23}\text{Na}$ reaction rate was mainly due to the poorly constrained contribution of a number of tentative low-energy resonances (Fig. 1) [20–22] and of the direct capture component [23,24].

In this context the direct measurements performed at the Laboratory for Underground Nuclear Astrophysics (LUNA)

[25] played a significant role: first, three resonances at proton energies of 156.2 , 189.5 , and 259.7 keV, in the laboratory, were observed for the first time [26–29], providing also information on their energy and γ -decay modes. New stringent upper limits were provided for the resonances at 71 , 105 , and 215 keV [26–29]. Then the S factor, $S(E)$, was measured down to unprecedented low energies [29].

In parallel to LUNA, independent studies at the over-ground TUNL, DRAGON, and HZDR facilities, using direct (TUNL, HZDR) and inverse (DRAGON) kinematics, also redetermined resonance strengths [30–33], and independently

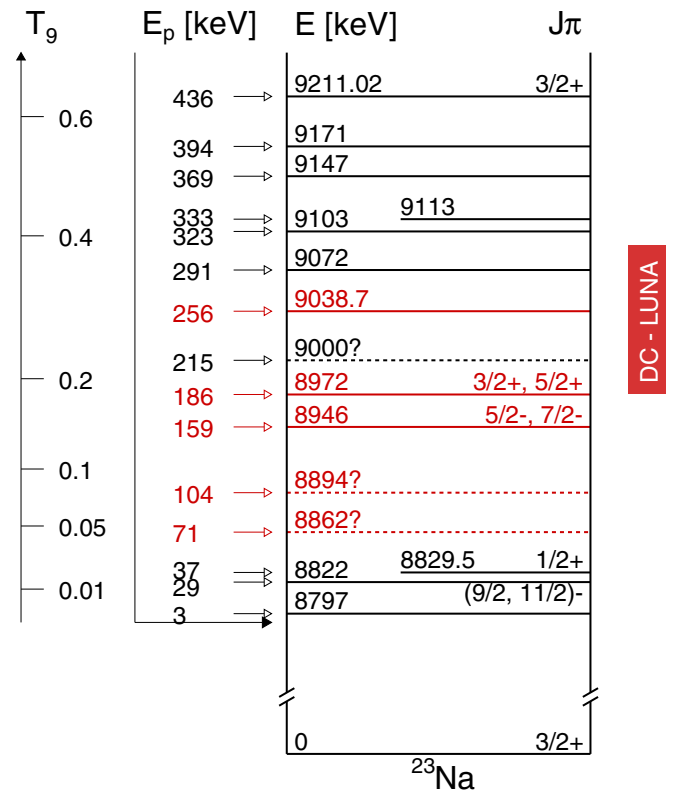


FIG. 1. Partial level scheme of ^{23}Na , with level energies taken from [35,36]. The energy range corresponding to the LUNA direct capture measurement [29, and present work] is indicated on the left in term of stellar temperature. The resonance energies in the laboratory system are shown together with the corresponding excited level energy and J^π . The resonances highlighted in red have been studied at LUNA [26,27,29, and present work].

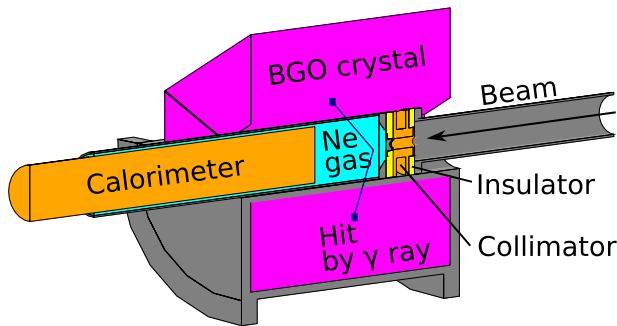


FIG. 2. Cross section of the experimental setup. More details are in the text and in [39].

reobserved several of the new resonances [31–33]. While overall there is a good agreement between results from different experiments concerning the resonance strengths, some tensions still remain on the branching ratios of the resonance γ -decay modes among Refs. [28,30,31]. Additionally, branching ratios are used for efficiency simulations and are of interest for the broader nuclear physics community.

A recent experiment, exploiting the proton inelastic-scattering reaction, combined with nonobservations of the 71, 105, and 215 keV resonance states in other experiments [26–29] ruled out the existence of these resonance states [34].

Regarding the cross section in the energy region away from the resonances, LUNA has reported results for the total S factor down to very low energies [29], i.e., $E_p \leq 400$ keV. In the energy region of overlap, DRAGON found total cross section values that agree with the LUNA results [33]. Direct capture cross sections were measured at higher energies by [23,24] and more recently by [31].

The aim of the present work is to determine new γ -decay branchings of the resonances at $E_p = 156.2$ and 259.7 keV and for the direct capture to different excited states of ^{23}Na , based on a refined reanalysis of data from Ref. [29]. These data may clarify existing discrepancies between reported branching ratios and aid in a comparison between γ -ray and recoil data. A new R -matrix fit of available data for the $^{22}\text{Ne}(p, \gamma)^{23}\text{Na}$ cross section and a revised reaction rate are provided, as well.

The paper is organized as follows: the experimental setup is described in Sec. II. Section III details the data analysis and experimental results for both the direct capture and the resonances. In Sec. IV, the calculation of the reaction rate is described and discussed. The summary and conclusion are given in Sec. V.

II. EXPERIMENTAL SETUP

The experimental setup was installed at the LUNA 400 kV accelerator [37] and it consisted of a cylindrical scattering chamber mounted in a windowless differential pumping system and filled with 2 mbar of ^{22}Ne gas; see [38,39] for a recent description of the LUNA gas target and Fig. 2 for a schematic view of the setup. The pumping system was operated in recirculation mode [39] and the ^{22}Ne gas (99.9% enrichment and 99.999% purity) was purified by a PS4-C3-R-2 heated getter

to remove nitrogen, oxygen, and carbohydrates. The nitrogen contamination was monitored by scanning the well known $E_p = 278$ keV resonance of $^{14}\text{N}(p, \gamma)^{15}\text{O}$ reaction on a daily basis [40–45]. Moreover to monitor the beam induced background, spectra were acquired filling the scattering chamber with argon. Proton capture reactions on argon are negligible at the LUNA 400 kV energies, and by properly setting the gas pressure it was possible to reproduce the same proton energy loss as in neon. During the argon monitor runs, the beam hits the collimator and the calorimeter, the two places where most contaminants are located, at the same energy as during the neon.

The beam current was determined to a precision of better than 1.5% by using a LABVIEW controlled calorimeter [39]. The target density along the scattering chamber and the beam heating correction were obtained with dedicated investigations, resulting in a final uncertainty on ^{22}Ne density profile of 1.3%, as detailed in [39].

A 4π BGO detector [46] surrounded the scattering chamber as shown in Fig. 2. The detector was composed of six optically independent sectors. The high Q value of the $^{22}\text{Ne}(p, \gamma)^{23}\text{Na}$ reaction and the extreme reduction of the cosmic ray radiation granted by the underground location of the LUNA 400 kV in the INFN Gran Sasso National Laboratories [25] allowed using the detector in adback mode, namely summing energies of coincident events in a $3.5 \mu\text{s}$ wide time window [47] from all segments as if the BGO were one single detector [48, and references therein]. The coincidence window was found as the optimal to distinguish true coincidences from both pile-up events and random signal-pulsar overlaps [47].

To characterize the BGO response two different simulation codes were implemented—GEANT3 [49] and GEANT4 [50] based, respectively—and validated using radioactive sources and the well known resonance at $E_p = 278$ keV in the $^{14}\text{N}(p, \gamma)^{15}\text{O}$ reaction [40–45]. The two codes were found to give consistent results and the overall efficiency uncertainty is 5%; see [29] for details.

III. DATA ANALYSIS AND RESULTS

Three low-energy peaks originating from the natural background, namely the $E_\gamma = 1461$, 2204, and 2614 keV peaks from the ^{40}K , ^{214}Bi , and ^{208}Tl decays, respectively, were used in the calibration procedure. These γ rays were always present in the spectra and clearly distinguishable in the ^{22}Ne runs. Due to the high Q value of the $^{22}\text{Ne}(p, \gamma)^{23}\text{Na}$ reaction, the calibration was extended by including the γ rays by the $^{14}\text{N}(p, \gamma)^{15}\text{O}$ aforementioned resonance and the $^{11}\text{B}(p, \gamma)^{12}\text{C}$ reaction, at energies around 11 and 16 MeV [51].

Once the single spectra were calibrated, the list-mode acquisition was exploited for the creation of the adback spectrum. The signals from the single crystals contributing to the sum peak ROI in the adback spectrum were selected and used to produce the so called gated spectrum [29,48, and references therein]. The same gate was applied to Ar spectra to establish the ratio between Compton background in the region of interest and the high-energy $^{11}\text{B}(p, \gamma)^{12}\text{C}$ peaks at 11–16

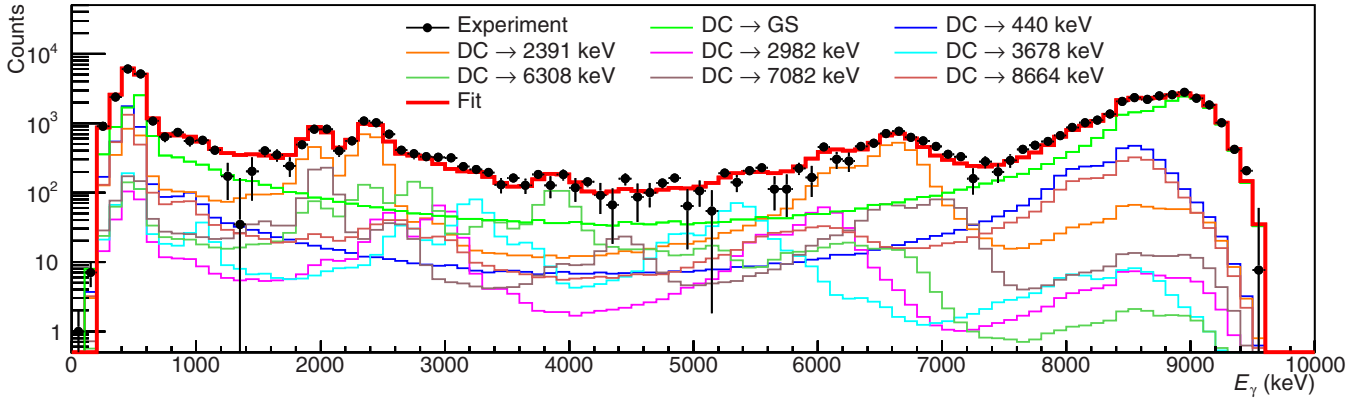


FIG. 3. Experimental spectrum at $E_{\text{eff}} = 306.2$ keV, gated at ROI = 8400–9600 keV, black points. Best fit simulated single cascades (colored lines) and their sum (red histogram) are shown for comparison.

MeV. This ratio was used for subtraction of the DC background in the gated neon spectra [29,39].

To access the branching ratios, the experimental net gated spectra were fitted with simulated templates, which were prepared for each resonance ($E_p = 156.2, 259.7$ keV) and for each nonresonant run ($E_p = 188, 205, 250,$ and 310 keV) separately. For each of these seven runs, a separate template was developed for the decay from the resonance, or the direct capture, to each accessible lower-lying state in ^{23}Na . The level scheme and decay branching ratios from the latest version of the Nuclear Data Sheets [52] was used for these templates. In the simulation, the trigger thresholds (each crystal was self-triggered with a threshold) and dead time were considered, as well as the energy straggling and energy loss of the proton beam inside the extended gas target [53,54].

During the fit, only the branching ratios of the primary γ rays under study here were considered free parameters, while all of the subsequent decays were fixed to the Nuclear Data Sheet values [52]. The TFractionFitter class of ROOT was used [55]. This class takes the statistical uncertainties of both the data and the Monte Carlo simulation into account. Finally, the effect of different starting parameter sets on the fit results, including possible false minima, was tested by repeating the

fit using a fine grid of starting parameters, and including also these effects in the error bar. The final branching ratio was given by the weighted average of these several fit results. The branching ratio error was typically dominated by the error due to this last step, not by the experimental or Monte Carlo statistics.

The aforementioned analysis routine was validated with the precise branching data of the $E_p = 278$ keV resonance in the $^{14}\text{N}(p, \gamma)^{15}\text{O}$ reaction [41], which were recovered within 4% discrepancy [53,54]. It must be noted that the detection efficiency for the sum peak in the addback spectrum depends on the branching ratios used in the simulations. However, their impact is mild, with a variation of the efficiency of less than 4% as a result of changing the primary branchings by 10%.

TABLE I. Average values and the adopted uncertainties for the direct capture (DC) branchings in the energy range 188–310 keV.

Final E_x (keV) [36,57]	DC fraction adopted (%)
0	48.1 ± 2.7
440.2(4)	9.8 ± 3.2
2390.9(3)	14.7 ± 3.6
2640.5(6)	< 1.5
2982.0(5)	2.4 ± 1.7
3677.9(5)	< 2.2
6305.6(6)	2.8 ± 2.2
6920.6(2)	< 2.2
7081.9(3)	< 3.4
8665.0(18)	11.2 ± 5.9
8826.5(19)	< 1.6

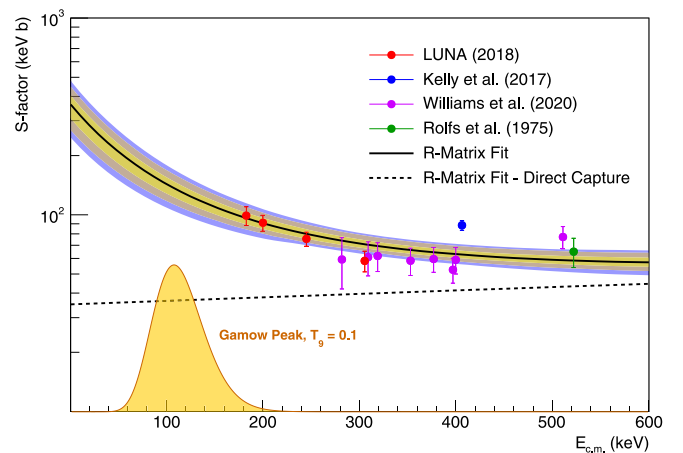


FIG. 4. The total S -factor data from LUNA, corrected for the screening effect [29], and from literature used in the R -matrix fit (black line). The three colored areas represent the $1\sigma, 2\sigma, 3\sigma$ regions of the fit; see text for details and Table I for adopted branchings of the cascades contributing to the total S factor. The dashed line is the direct capture component as resulting from the R -matrix fit. A comparison between this work and the previously estimated direct capture contribution, $S_{\text{DC}}(0)$, is in Table II.

TABLE II. Extrapolated S factor for the direct capture component only, $S_{\text{DC}}(0)$, from the literature and the present work. It must be noted that direct capture is treated as dependent on energy only in the present analysis, while in literature it was assumed constant.

$S_{\text{DC}}(0)$ (keV b)	Source
67 ± 12	C. Rolfs <i>et al.</i> [24]
62	J. Goerres <i>et al.</i> [23]
48.8 ± 9.5	R. Santra <i>et al.</i> [59]
60	M. Williams <i>et al.</i> [33]
50 ± 12	F. Ferraro <i>et al.</i> [29]
35 ± 5	Present work

A. Direct capture

The nonresonant component of the $^{22}\text{Ne}(p, \gamma)^{23}\text{Na}$ cross section was determined experimentally by Rolfs *et al.* [24] and by Görres *et al.* [23] at energies $E_p > 500$ keV, resulting in an extrapolated $S_{\text{DC}}(0) = 67(12)$ and 62 keV b, respectively. Görres *et al.* [23] also measured the cross section of the ground state capture down to $E_p = 287$ keV, finding that its low-energy trend is affected by both the contribution of the subthreshold resonance at $E_p = -135$ keV and the resonance at $E_p = 38$ keV, which decay to the ground state with 84% and 36% probabilities, respectively. Therefore, extrapolations of the cross section to zero energy heavily rely on the subthreshold resonance parameters.

In the present study, the intensities of the direct capture to ten different excited states of ^{23}Na and the ground state were determined at four energies in the range $E_p = 188$ –310 keV, far off the energies of known or supposed narrow resonances. These new data cover an energy domain that was previously unexplored. While here we provide transition prob-

abilities to individual excited states, the results on the total cross section are reported in [29]. As an example of the fitting procedure, the gated spectrum for the effective energy $E_{\text{eff}} = 306.2$ keV, namely the cross-section-weighted average energy integrated over the target thickness [56], with the simulated templates used in the fit, is shown in Fig. 3. None of the branching ratios obtained show variations as a function of beam energy in the energetic range explored here, so we averaged the branching ratios obtained at different beam energies. The results are reported in Table I. A conservative approach was used for the uncertainty estimation, adopting the maximum deviation between the average and the branchings measured at different energies. For some of the transitions only an upper limit is reported, obtained by averaging the values derived at different proton energies.

The DRAGON Collaboration reported eight data points for the cross section [32,33] in an energy range above the LUNA data, but with a small overlap, as shown in Fig. 4. Their dataset is in excellent agreement with LUNA data [29], which are corrected for the screening effect via the adiabatic approach [58], but with slightly higher uncertainties. Since DRAGON studied also the resonance at $E_p = 479$ keV, they performed a re-normalization of the single TUNL data point at $E_p = 425$ keV [31], which was found to be in better agreement with the DRAGON S -factor values and also with the trend reported in [29]. In order to better constrain the trend of the direct capture contribution and to properly fix the subthreshold resonance shape at very low energies, we included the recent DRAGON results in the present reevaluation of the nonresonant contribution via R -matrix fit, which supersedes the previous evaluation in [29].

The R -matrix fit was performed through the AZURE2 code and all the subthreshold states were considered with their ANC parameters taken from [59]. For the $E_x = 8665$ keV

TABLE III. Decay branching ratios for the three resonances of $^{22}\text{Ne}(p, \gamma)^{23}\text{Na}$ observed in the present experiment and reported in LUNA-HPGe [28], TUNL [31], and Jenkins [36].

E_x (keV)	Branching ratios (%)								
	$E_p^{\text{res}} = 156.2$ keV				$E_p^{\text{res}} = 189.5$ keV			$E_p^{\text{res}} = 259.7$ keV	
	Jenkins	TUNL	LUNA HPGe	This work	TUNL	LUNA HPGe	[39]	LUNA HPGe	This work
g.s.					5.3 ± 1.4		≤ 1		
440					37.7 ± 1.5	42.8 ± 0.9	35 ± 6	45.4 ± 0.9	44.8 ± 1.4
2076					39.8 ± 1.3	47.9 ± 0.9	53 ± 6	18.7 ± 0.6	17.9 ± 0.4
2391	39 ± 6	20 ± 4	23 ± 4	33.5 ± 1.8					
2704								10.9 ± 0.5	14.0 ± 0.3
2982					5.0 ± 0.8	3.7 ± 0.5	3.3 ± 0.7		
3678					2.2 ± 0.8		2.4 ± 0.5		
3848								13.3 ± 0.5	14.7 ± 0.4
3915	61 ± 30	80 ± 6	77 ± 4	66.5 ± 2.2	3.1 ± 0.6	1.1 ± 0.3	1.6 ± 0.5	1.8 ± 0.4	0.8 ± 0.2
4775					≤ 3.0	1.8 ± 0.2	1.9 ± 0.4		
5927								3.6 ± 0.2	2.7 ± 0.4
6042								2.6 ± 0.2	1.5 ± 0.7
6355								1.5 ± 0.2	2.2 ± 0.3
6618					4.7 ± 0.9	2.7 ± 0.2	2.5 ± 0.8		
6820								2.2 ± 0.2	1.5 ± 0.4

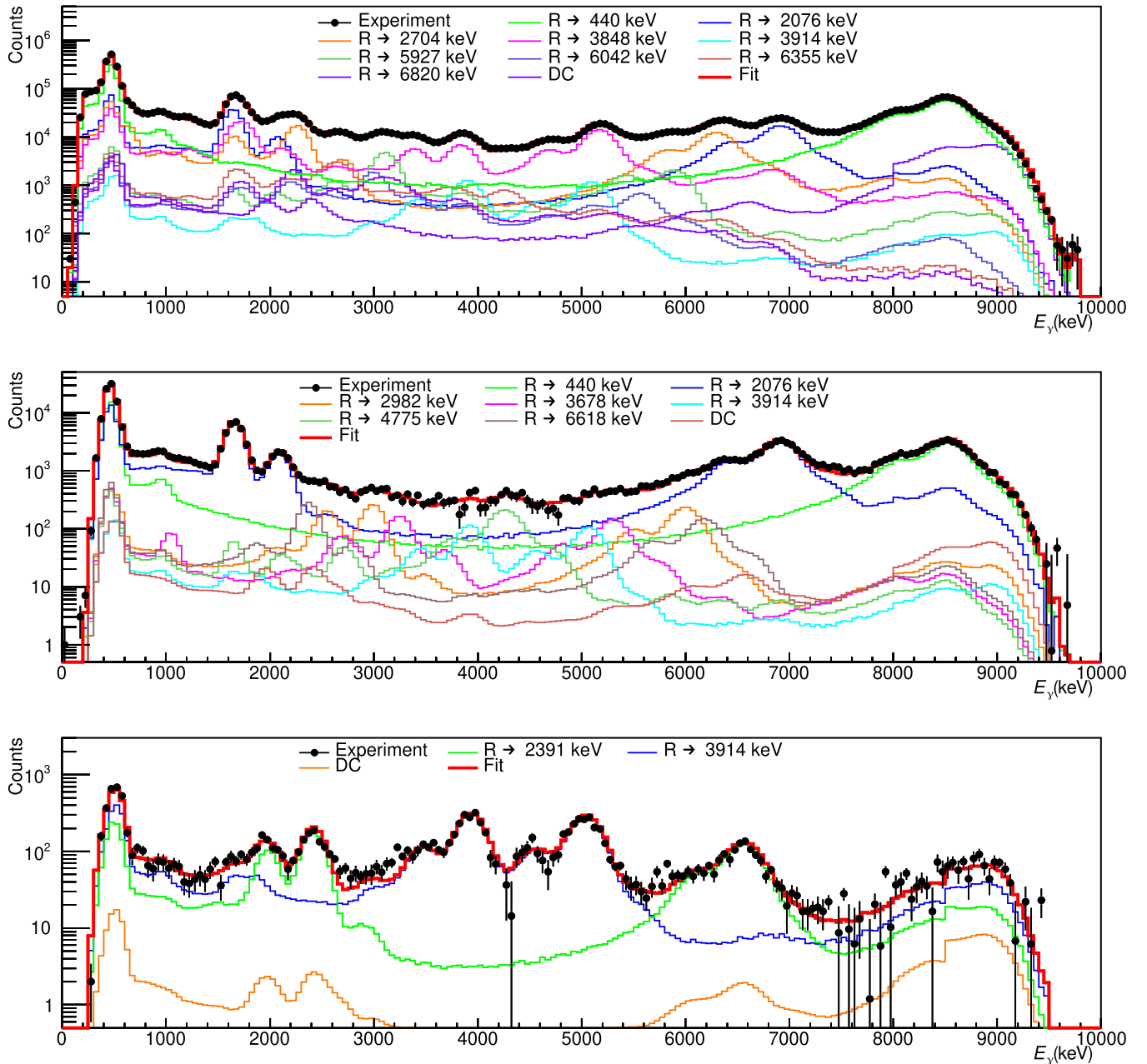


FIG. 5. Experimental spectra of the resonances at, from top to bottom, $E_p = 259.7, 156.2,$ and 189.5 keV (from [39]), gated at ROI = 8000–9800, 7700–9700, and 8400–9500 keV, respectively.

state a radiative width was added as well, since it could impact the extrapolation at lowest energies. The $1/2^-$, $1/2^+$, and $3/2^-$ background poles were also included. To perform the minimization, the Bayesian approach was followed with the use of the emcee library [60] and the BRICK package [61]. The prior distributions for the ANCs were considered as normal functions with the width given by their respective uncertainties. The normalization factors for each dataset were left free and their priors were assumed as normal distributions, with the width defined by the reported systematic uncertainty. For all the other parameters, so-called flat priors (flat probability density functions) within set limits, were used. See the Supplemental Material [62] for a list of the R -matrix fit inputs.

The resulting extrapolation for the total S factor is shown in Fig. 4, solid line, together with literature data. The obtained value for $S(0)$ is 0.36 ± 0.05 MeV b. In Fig. 4, the dashed line indicates the present direct capture component, which was treated following the prescriptions in [63] for the energy dependence. In Table II the present direct component extrapolation, $S_{DC}(0)$, is compared to literature data, obtained considering the nonresonant contribution constant with the energy.

B. Resonances

Here we report the new results for the branching ratio of the 156.2 and 259.7 keV resonance cascades, as obtained by

TABLE IV. The $^{22}\text{Ne}(p, \gamma)^{23}\text{Na}$ resonance strengths adopted here. For the reaction rate calculation a screening correction was applied to resonances studied at LUNA; see text for details. Upper limits from [29] are given at 90% confidence level. Resonances at $E_p > 661$ keV are adopted without change from Ref. [18] but are not listed here.

E_p^{res} (keV)	Strength $\omega\gamma$ (eV)				f
	Literature direct	Literature indirect	LUNA [26,29]	Adopted	
29		$\leq 3.2 \times 10^{-25}$ [21]		$\leq 2.6 \times 10^{-25}$	
37		$\leq 2.6 \times 10^{-25}$ [65]			
		3.6×10^{-15} [21]		$(3.1 \pm 1.2) \times 10^{-15}$	
		$(3.1 \pm 1.2) \times 10^{-15}$ [65]			
71	$\leq 3.2 \times 10^{-6}$ [22]	$\leq 1.9 \times 10^{-10}$ [21]	$\leq 6 \times 10^{-11}$		
105	$\leq 0.6 \times 10^{-6}$ [22]	$\leq 1.4 \times 10^{-7}$ [21]	$\leq 7 \times 10^{-11}$		
156.2	$\leq 1.0 \times 10^{-6}$ [22]	9.2×10^{-9} [21]	$(2.2 \pm 0.2) \times 10^{-7}$	$(2.2 \pm 0.2) \times 10^{-7}$	1.07
	$(2.03 \pm 0.40) \times 10^{-7}$ [31]	$(9.2 \pm 3.7) \times 10^{-9}$ [65]			
	$1.7_{-0.4}^{+0.5} \times 10^{-7}$ [32,33]				
189.5	$\leq 2.6 \times 10^{-6}$ [22]	3.4×10^{-6} [21]	$(2.7 \pm 0.2) \times 10^{-6}$	$(2.7 \pm 0.2) \times 10^{-6}$	1.06
	$(2.32 \pm 0.32) \times 10^{-6}$ [31]				
	$(2.2 \pm 0.4) \times 10^{-6}$ [32,33]				
215	$\leq 1.4 \times 10^{-6}$ [22]		$\leq 2.8 \times 10^{-8}$		
259.7	$\leq 2.6 \times 10^{-6}$ [22]	$\leq 1.3 \times 10^{-7}$ [21]	$(9.7 \pm 0.7) \times 10^{-6}$	$(9.7 \pm 0.7) \times 10^{-6}$	1.03
	$(8.5 \pm 1.4) \times 10^{-6}$ [32,33]				
291	$\leq 2.2 \times 10^{-6}$ [22]			$\leq 2.2 \times 10^{-6}$	
323	$\leq 2.2 \times 10^{-6}$ [22]			$\leq 2.2 \times 10^{-6}$	
334	$\leq 3.0 \times 10^{-6}$ [22]			$\leq 3.0 \times 10^{-6}$	
369		$\leq 6.0 \times 10^{-4}$ [21]		$\leq 6.0 \times 10^{-4}$	
394		$\leq 6.0 \times 10^{-4}$ [21]		$\leq 6.0 \times 10^{-4}$	
436	(0.079 ± 0.006) [30]			(0.079 ± 0.006)	
	(0.088 ± 0.01) [31]				
479	(0.594 ± 0.038) [30]			(0.594 ± 0.038)	
	(0.583 ± 0.043) [66]				
	(0.44 ± 0.02) [32,33]				
638.5	(2.45 ± 0.18) [30]			(2.45 ± 0.18)	
	(2.6 ± 0.3) [33]				
661	(0.032 ± 0.017) [30]			(0.032 ± 0.015)	
	(0.45 ± 0.03) [33]				

fitting LUNA data in [29] as described in Sec. III. In the following, results are discussed and compared with literature data while they are summarized in Table III. Moreover we include more details of the analysis performed for the branching ratio determination of the 189.5 keV resonance, whose results are published in [39].

C. 259.7 keV resonance ($E_x = 9042.4$ keV)

The resonance at 259.7 keV corresponds to the $E_x = 9042.4$ keV excited state in ^{23}Na . This level was reported as part of a doublet with the 9038 keV level in [36]. According to [36], the 9038 keV level has $J^\pi = 15/2^+$, while $J^\pi = 7/2^+$ or $9/2^+$ was assigned to the 9042.4 keV level. None of the transitions reported in [36] for the 9038 keV level have been observed in the present work, probably as consequence of the high angular momentum of the level. The branching ratios obtained in this work are in Fig. 5 (top panel) and in Table III. An overall agreement with previous LUNA results is evident, except for the transition to the 2704 keV level. This resonance was recently studied by the DRAGON Collaboration [32,33], resulting in a resonance strength 1σ compatible with the value reported in [29]; see Table IV.

D. 189.5 keV resonance ($E_x = 8975.3$ keV)

The 189.5 keV resonance corresponds to the 8975.3 keV excited state in ^{23}Na with spin-parity $5/2^+$ [31,35].

The branching ratios reported in [39], as derived from the best fit reported here in Fig. 5 (middle panel) are compared with literature results [28,31] in Table III. It must be noted that in the minimization procedure the branching ratio sets from [28] and [31] were also considered; however, they were unable to reproduce the experimental spectrum [39]. In particular the transition to the ground state claimed in [31] is not confirmed here [39].

Recently DRAGON reported for this resonance a new resonance strength [32,33] compatible with results in literature [29,31]; see Table IV.

E. 156.2 keV resonance ($E_x = 8943.5$ keV)

The 156.2 keV resonance corresponds to the 8943.5 keV excitation energy in ^{23}Na , which is reported as a doublet by [36] with one level having $J^\pi = 7/2^-$, while the other a tentatively assigned $3/2^+$. As a matter of fact, for the low proton beam energies used here, the $7/2^-$ level is strongly disfavored by the angular momentum barrier. Primary transitions to the

TABLE V. The presently adopted thermonuclear reaction rate (median rate) for the $^{22}\text{Ne}(p, \gamma)^{23}\text{Na}$ reaction in units $\text{cm}^{-3}\text{s}^{-1}\text{mol}^{-1}$, as a function of temperature T_9 in GK units. The low and high rates were obtained by subtracting and adding 1σ uncertainty, respectively.

T_9	Low rate	Median rate	High rate
0.01	2.76×10^{-25}	6.97×10^{-25}	1.65×10^{-24}
0.011	1.06×10^{-23}	2.53×10^{-23}	5.63×10^{-23}
0.012	2.21×10^{-22}	4.99×10^{-22}	1.05×10^{-21}
0.013	2.85×10^{-21}	5.91×10^{-21}	1.25×10^{-20}
0.014	2.53×10^{-20}	5.28×10^{-20}	1.03×10^{-19}
0.015	1.66×10^{-19}	3.38×10^{-19}	6.39×10^{-19}
0.016	8.57×10^{-19}	1.70×10^{-18}	3.14×10^{-18}
0.018	1.30×10^{-17}	2.49×10^{-17}	4.36×10^{-17}
0.02	1.12×10^{-16}	2.09×10^{-16}	3.53×10^{-16}
0.025	5.16×10^{-15}	9.15×10^{-15}	1.46×10^{-14}
0.03	6.25×10^{-14}	1.08×10^{-13}	1.65×10^{-13}
0.04	1.29×10^{-12}	2.17×10^{-12}	3.19×10^{-12}
0.05	7.50×10^{-12}	1.24×10^{-11}	1.77×10^{-11}
0.06	2.64×10^{-11}	4.19×10^{-11}	5.82×10^{-11}
0.07	1.13×10^{-10}	1.57×10^{-10}	2.02×10^{-10}
0.08	8.59×10^{-10}	1.05×10^{-9}	1.25×10^{-9}
0.09	6.60×10^{-9}	7.73×10^{-9}	8.91×10^{-9}
0.1	3.83×10^{-8}	4.42×10^{-8}	5.04×10^{-8}
0.11	1.69×10^{-7}	1.94×10^{-7}	2.19×10^{-7}
0.12	5.95×10^{-7}	6.77×10^{-7}	7.65×10^{-7}
0.13	1.74×10^{-6}	1.98×10^{-6}	2.23×10^{-6}
0.14	4.42×10^{-6}	5.00×10^{-6}	5.62×10^{-6}
0.15	9.94×10^{-6}	1.12×10^{-5}	1.26×10^{-5}
0.16	2.03×10^{-5}	2.29×10^{-5}	2.56×10^{-5}
0.18	6.76×10^{-5}	7.61×10^{-5}	8.50×10^{-5}
0.2	1.83×10^{-4}	2.06×10^{-4}	2.30×10^{-4}
0.25	1.81×10^{-3}	2.00×10^{-3}	2.24×10^{-3}
0.3	2.15×10^{-2}	2.34×10^{-2}	2.58×10^{-2}
0.35	1.76×10^{-1}	1.90×10^{-1}	2.08×10^{-1}
0.4	9.01×10^{-1}	9.71×10^{-1}	1.05×10^0
0.45	3.23×10^0	3.48×10^0	3.76×10^0
0.5	8.97×10^0	9.66×10^0	1.04×10^1
0.6	4.16×10^1	4.49×10^1	4.85×10^1
0.7	1.25×10^2	1.36×10^2	1.47×10^2
0.8	2.88×10^2	3.17×10^2	3.46×10^2
0.9	5.57×10^2	6.20×10^2	6.84×10^2
1.0	9.52×10^2	1.08×10^3	1.20×10^3

3915 and 2391 keV states have been observed in this work (Fig. 5, bottom panel) as well as in previous experiments [28,31,36]; see Table III.

The resonance strengths provided by recent measurements are in agreement within 1σ [29,31,32]; see Table IV.

IV. REACTION RATE

The present extrapolation for the total cross section (Fig. 4) was used to calculate a new reaction rate, reported in Table V. All the previously reported narrow resonances were added by

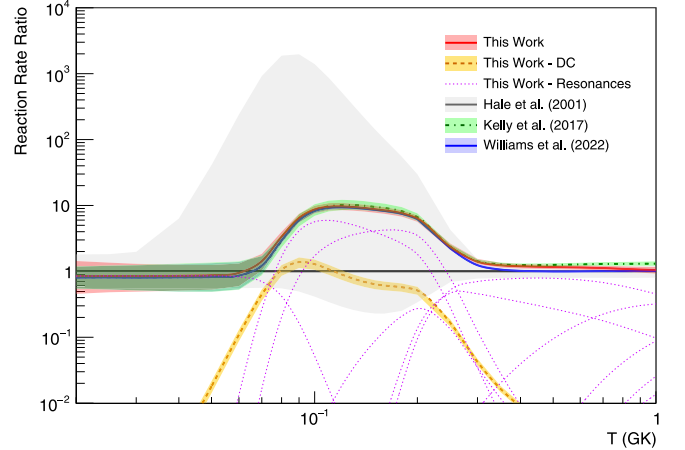


FIG. 6. The present $^{22}\text{Ne}(p, \gamma)^{23}\text{Na}$ total reaction rate and others from literature [21,31,33] are shown normalized to [21] and with error bands corresponding to 1σ . The contribution of individual resonances (contributing more than 1% to the total rate) is given in magenta. The DC component is shown in dashed orange line with relative error as from the R -matrix fit.

using the following approximation:

$$R_i = \frac{1.54 \times 10^{11}}{T_9^{3/2}} \left(\frac{M_p + M_{22}}{M_p M_{22}} \right)^{3/2} \omega \gamma_i \exp \left(-11.605 \frac{E_i}{T_9} \right), \quad (1)$$

where T_9 is the temperature in GK, M_p and M_{22} are the proton and ^{22}Ne masses in amu, respectively, and E_i is the center-of-mass energy of the resonance. Resonance strengths, $\omega \gamma_i$, and energies, E_i , assumed here are given in Table IV. Following the prescriptions in [58], the screening correction factors, f , were estimated between 1.07 and 1.03 for the resonances investigated by LUNA; see Table IV. A recently published approach suggests that the screening correction in case of narrow resonances is negligible [64]. The new formalism, however, is still under debate.

For the resonances for which only upper limits are reported the formalism described in [28] was used. Resonances at 71, 105, and 215 keV were not considered [34].

The final rate is shown in Fig. 6 and compared with the most recent results in literature and with the commonly adopted rate from [21]. Over the whole temperature range in Fig. 6 the present rate uncertainty is reduced compared to the result in [21]. At $0.02 \leq T \leq 0.15$ GK the present uncertainty is compatible with [31,33] and strongly reduced compared to a previous LUNA rate [29], because of the different treatment of 71 and 105 keV resonances. The new reaction rate is in good agreement with literature results, except at $0.09 \leq T \leq 0.3$ GK, where it is up to 30% higher than the most adopted rate [21], as a consequence of the improved resonance contribution estimation.

V. SUMMARY AND OUTLOOK

The total S -factor of the $^{22}\text{Ne}(p, \gamma)^{23}\text{Na}$ reaction was recently measured by LUNA down to the lowest energy to date. From the same measurement we reported here the results for

the branching ratio of direct capture to different excited states of ^{23}Na . Moreover, we propose an updated extrapolation for the total S factor and for the direct capture component based on a dedicated R -matrix fit of LUNA data and recent results reported in literature. New γ -decay branchings are provided for the resonances at 156.2 and 259.7 keV. An overall good agreement is found with respect to previous LUNA and literature results. A new reaction rate was calculated based on the present results and recently published data and can be adopted for future investigation of AGB star nucleosynthesis and its impact on the abundance anomalies in globular clusters.

ACKNOWLEDGMENTS

D. Ciccotti and the technical staff of the LNGS are gratefully acknowledged for their help during setup, construction,

and data taking. Financial support by INFN, the Italian Ministry of Education, University and Research (MIUR) through the Dipartimenti di Eccellenza and FARE-EASy project “Science of the Universe,” the European Union (ERC Consolidator Grant Projects STARKEY No. 615604, ERC-StG SHADES No. 852016, and ChETEC-INFRA No. 101008324), Deutsche Forschungsgemeinschaft (DFG, BE 4100-4/1), the Helmholtz Association (ERC-RA-0016), the Hungarian National Research, Development and Innovation Office (NKFIH K134197, PD129060 and FK134845), the European Collaboration for Science and Technology (COST Action ChETEC, CA16117), and DAAD fellowships at HZDR for the authors F.C., R.D., and D.P. are gratefully acknowledged. The authors C.G.B., R.S.S., T.D., and M.A. acknowledge funding by STFC UK (Grant No. ST/L005824/1).

-
- [1] M. Forestini and C. Charbonnel, *Astron. Astrophys. Suppl. Ser.* **123**, 241 (1997).
- [2] J. José and M. Hernanz, *Astrophys. J.* **494**, 680 (1998).
- [3] R. G. Izzard, M. Lugaro, A. I. Karakas, C. Iliadis, and M. van Raai, *Astron. Astrophys.* **466**, 641 (2007).
- [4] R. G. Gratton, E. Carretta, and A. Bragaglia, *Astron. Astrophys. Rev.* **20**, 50 (2012).
- [5] R. Gratton, A. Bragaglia, E. Carretta, V. D’Orazi, S. Lucatello, and A. Sollima, *Astron. Astrophys. Rev.* **27**, 8 (2019).
- [6] G. Piotto, L. R. Bedin, J. Anderson, I. R. King, S. Cassisi, A. P. Milone, S. Villanova, A. Pietrinfermi, and A. Renzini, *Astrophys. J.* **661**, L53 (2007).
- [7] S. Villanova, G. Piotto, I. R. King, J. Anderson, L. R. Bedin, R. G. Gratton, S. Cassisi, Y. Momany, A. Bellini, A. M. Cool, A. Recio-Blanco, and A. Renzini, *Astrophys. J.* **663**, 296 (2007).
- [8] R. G. Gratton, P. Bonifacio, A. Bragaglia, E. Carretta, V. Castellani, M. Centurion, A. Chieffi, R. Claudi, G. Clementini, F. D’Antona, S. Desidera, P. François, F. Grundahl, S. Lucatello, P. Molaro, L. Pasquini, C. Sneden, F. Spite, and O. Straniero, *Astron. Astrophys.* **369**, 87 (2001).
- [9] J.-W. Lee, *Mon. Not. R. Astron. Soc. Lett.* **405**, L36 (2010).
- [10] F. D’Antona, E. Vesperini, A. D’Ercole, P. Ventura, A. P. Milone, A. F. Marino, and M. Tailo, *Mon. Not. R. Astron. Soc.* **458**, 2122 (2016).
- [11] R. G. Izzard, S. E. de Mink, O. R. Pols, N. Langer, H. Sana, and A. de Koter, *Mem. Soc. Astron. Ital.* **84**, 171 (2013).
- [12] M. Krause, C. Charbonnel, T. Decressin, G. Meynet, and N. Prantzos, *Astron. Astrophys.* **552**, A121 (2013).
- [13] P. A. Denissenkov and F. D. A. Hartwick, *Mon. Not. R. Astron. Soc. Lett.* **437**, L21 (2013).
- [14] D. Geisler, S. Villanova, G. Carraro, C. Pilachowski, J. Cummings, C. I. Johnson, and F. Bresolin, *Astrophys. J. Lett.* **756**, L40 (2012).
- [15] A. Slemer *et al.*, *Mon. Not. R. Astron. Soc.* **465**, 4817 (2017).
- [16] M. Wang, W. Huang, F. Kondev, G. Audi, and S. Naimi, *Chin. Phys. C* **45**, 030003 (2021).
- [17] C. Angulo *et al.*, *Nucl. Phys. A* **656**, 3 (1999).
- [18] A. L. Sallaska, C. Iliadis, A. E. Champagne, S. Goriely, S. Starrfield, and F. X. Timmes, *Astrophys. J. Suppl. Ser.* **207**, 18 (2013).
- [19] C. Iliadis, A. Champagne, J. José, S. Starrfield, and P. Tupper, *Astrophys. J. Suppl. Ser.* **142**, 105 (2002).
- [20] J. R. Powers, H. T. Fortune, R. Middleton, and O. Hansen, *Phys. Rev. C* **4**, 2030 (1971).
- [21] S. E. Hale, A. E. Champagne, C. Iliadis, V. Y. Hansper, D. C. Powell, and J. C. Blackmon, *Phys. Rev. C* **65**, 015801 (2001).
- [22] J. Görres, C. Rolfs, P. Schmalbrock, H. P. Trautvetter, and J. Keinonen, *Nucl. Phys. A* **385**, 57 (1982).
- [23] J. Görres, H. W. Becker, L. Buchmann, C. Rolfs, P. Schmalbrock, H. P. Trautvetter, A. Vlieks, J. W. Hammer, and T. R. Donoghue, *Nucl. Phys. A* **408**, 372 (1983).
- [24] C. Rolfs, W. S. Rodney, M. H. Shapiro, and H. Winkler, *Nucl. Phys. A* **241**, 460 (1975).
- [25] M. Aliotta, A. Boeltzig, R. Depalo, and G. Gyürky, *Annu. Rev. Nucl. Part. Sci.* **72**, 177 (2022).
- [26] F. Cavanna *et al.*, *Phys. Rev. Lett.* **115**, 252501 (2015).
- [27] F. Cavanna, R. Depalo, M. Aliotta, M. Anders, D. Bemmerer, A. Best, A. Boeltzig, C. Broggini, C. G. Bruno, A. Caciolli, P. Corvisiero, T. Davinson, A. diLeva, Z. Elekes, F. Ferraro, A. Formicola, Z. Fulop, G. Gervino, A. Guglielmetti, C. Gustavino *et al.*, *Phys. Rev. Lett.* **120**, 239901(E) (2018).
- [28] R. Depalo *et al.*, *Phys. Rev. C* **94**, 055804 (2016).
- [29] F. Ferraro *et al.*, *Phys. Rev. Lett.* **121**, 172701 (2018).
- [30] R. Depalo *et al.*, *Phys. Rev. C* **92**, 045807 (2015).
- [31] K. J. Kelly, A. E. Champagne, L. N. Downen, J. R. Dermigny, S. Hunt, C. Iliadis, and A. L. Cooper, *Phys. Rev. C* **95**, 015806 (2017).
- [32] A. Lennarz *et al.*, *Phys. Lett. B* **807**, 135539 (2020).
- [33] M. Williams *et al.*, *Phys. Rev. C* **102**, 035801 (2020).
- [34] D. P. Carrasco-Rojas, M. Williams, P. Adsley, L. Lamia, B. Bastin, T. Faestermann, C. Fougères, F. Hammache, D. S. Harrouz, R. Hertenberg, M. La Cognata, A. Meyer, F. de Oliveira Santos, S. Palmerini, R. G. Pizzone, S. Romano, N. de Séréville, A. Tumino, and H. F. Wirth, *Phys. Rev. C* **108**, 045802 (2023).
- [35] R. B. Firestone, *Nucl. Data Sheets* **108**, 1 (2007).
- [36] D. G. Jenkins, M. Bouhelal, S. Courtin, M. Freer, B. R. Fulton, F. Haas, R. V. F. Janssens, T. L. Khoo, C. J. Lister, E. F. Moore, W. A. Richter, B. Truett, and A. H. Wuosmaa, *Phys. Rev. C* **87**, 064301 (2013).

- [37] A. Formicola *et al.*, *Nucl. Instrum. Methods A* **507**, 609 (2003).
- [38] V. Mossa *et al.*, *Eur. Phys. J. A* **56**, 144 (2020).
- [39] F. Ferraro *et al.*, *Eur. Phys. J. A* **54**, 44 (2018).
- [40] G. Gyürky, Z. Halász, G. G. Kiss, T. Szücs, A. Csík, Z. Török, R. Huszánk, M. G. Kohan, L. Wagner, and Z. Fülöp, *Phys. Rev. C* **100**, 015805 (2019).
- [41] S. Daigle, K. J. Kelly, A. E. Champagne, M. Q. Buckner, C. Iliadis, and C. Howard, *Phys. Rev. C* **94**, 025803 (2016).
- [42] D. Bemmerer, *Nucl. Phys. A* **779**, 297 (2006).
- [43] G. Imbriani, H. Costantini, A. Formicola, A. Vomiero, C. Angulo, D. Bemmerer, R. Bonetti, C. Brogini, F. Confortola, P. Corvisiero, J. Cruz, P. Descouvemont, Z. Fülöp, G. Gervino, A. Guglielmetti, C. Gustavino, G. Gyürky, A. P. Jesus, M. Junker, J. N. Klug *et al.*, *Eur. Phys. J. A* **25**, 455 (2005).
- [44] R. C. Runkle, A. E. Champagne, C. Angulo, C. Fox, C. Iliadis, R. Longland, and J. Pollanen, *Phys. Rev. Lett.* **94**, 082503 (2005).
- [45] H. W. Becker, W. E. Kieser, C. Rolfs, H. P. Trautvetter, and M. Wiescher, *Z. Phys. A* **305**, 319 (1982).
- [46] C. Casella *et al.*, *Nucl. Instrum. Methods Phys. Res. Sect. A* **489**, 160 (2002).
- [47] A. Boeltzig *et al.*, *J. Phys. G: Nucl. Part. Phys.* **45**, 025203 (2018).
- [48] J. Skowronski *et al.*, *J. Phys. G: Nucl. Part. Phys.* **50**, 045201 (2023).
- [49] R. Brun, F. Bruyant, F. Carminati, S. Giani, M. Maire, A. McPherson, G. Patrick, and L. Urban, *GEANT Detector Description and Simulation Tool*, Technical Report (CERN, Geneva, 1994).
- [50] S. Agostinelli *et al.*, *Nucl. Instrum. Methods Phys. Res. Sect. A* **506**, 250 (2003).
- [51] J. H. Kelley, J. E. Purcell, and C. G. Sheu, *Nucl. Phys. A* **968**, 71 (2017).
- [52] M. Shamsuzzoha Basunia and A. Chakraborty, *Nucl. Data Sheets* **171**, 1 (2021).
- [53] F. Ferraro, Direct measurement of the $^{22}\text{Ne}(p, \gamma)^{23}\text{Na}$ reaction cross section at astrophysical energies, Ph.D. thesis, Università degli Studi di Genova, 2017.
- [54] M. P. Takács, Hydrogen burning: Study of the $^{22}\text{Ne}(p, \gamma)^{23}\text{Na}$, $^3\text{He}(\alpha, \gamma)^7\text{Be}$ and $^7\text{Be}(p, \gamma)^8\text{B}$ reactions at ultra-low energies, Ph.D. thesis, Technische Universität Dresden, 2017.
- [55] R. Barlow and C. Beeston, *Comput. Phys. Commun.* **77**, 219 (1993).
- [56] C. R. Brune and D. B. Sayre, *Nucl. Instrum. Methods Phys. Res. Sect. A* **698**, 49 (2013).
- [57] M. Wang, G. Audi, F. G. Kondev, W. J. Huang, S. Naimi, and X. Xu, *Chin. Phys. C* **41**, 030003 (2017).
- [58] H. J. Assenbaum, K. Langanke, and C. Rolfs, *Z. Phys. A* **327**, 461 (1987).
- [59] R. Santra, S. Chakraborty, and S. Roy, *Phys. Rev. C* **101**, 025802 (2020).
- [60] D. Foreman-Mackey, D. W. Hogg, D. Lang, and J. Goodman, *Publ. Astron. Soc. Pac.* **125**, 306 (2013).
- [61] D. Odell, C. R. Brune, D. R. Phillips, R. J. deBoer, and S. N. Paneru, *Front. Phys.* **10**, 888476 (2022).
- [62] See Supplemental Material at <http://link.aps.org/supplemental/10.1103/PhysRevC.109.064627> for Azure2 input file for the present R-matrix fit.
- [63] P. Descouvemont and D. Baye, *Rep. Prog. Phys.* **73**, 036301 (2010).
- [64] C. Iliadis, *Phys. Rev. C* **107**, 044610 (2023).
- [65] C. Iliadis, R. Longland, A. E. Champagne, and A. Coc, *Nucl. Phys. A* **841**, 251 (2010).
- [66] K. J. Kelly, A. E. Champagne, R. Longland, and M. Q. Buckner, *Phys. Rev. C* **92**, 035805 (2015).